

Analysis of Corrosion Behavior and Surface Properties of Plasma-Sprayed HA/Ta Coating on CoCr Alloy

Balraj Singh¹ · Gurpreet Singh¹ · Buta Singh Sidhu²

Submitted: 17 June 2018 / in revised form: 25 September 2018 / Published online: 12 November 2018
© ASM International 2018

Abstract The cobalt–chromium (CoCr) alloys have been extensively used as implants, especially in total joint replacements and in odontology, due to their superior mechanical properties and wear resistance in vivo. However, the excessive release of the ‘Co’ and ‘Cr’ ions from CoCr implants can lead to adverse health issues, such as hypersensitivity and inflammatory reactions. The present study aimed to improve the corrosion resistance of a medical grade CoCr alloy (ASTM F-1537) plasma-sprayed with tantalum (Ta)-reinforced hydroxyapatite (HA) coating. The weight percent (wt.%) of Ta content in HA coating was varied at three levels, i.e., 10, 20, and 30%. In vitro corrosion behavior was investigated by electrochemical measurements in Ringer’s solution along with surface properties analysis. The results revealed an increase in surface hardness value with an incremental increase in Ta content in the HA coating. The surface of HA as well as Ta-reinforced HA coatings possessed adequate roughness and demonstrated hydrophilic nature. With the Ta reinforcement in HA coating, the E_{corr} values shifted toward nobler potentials and I_{corr} values declined noticeably which indicated an increase in corrosion resistance of the surface. The results of the study indicate that the proposed Ta reinforcement in HA is potentially important for CoCr bio-implant applications.

Keywords implants · cobalt–chromium · corrosion · hydroxyapatite · plasma spray · tantalum

Introduction

Medical and surgical therapies have been progressed immensely due to the extensive research. However, despite the advancements, such as advances in suppressive antimicrobial therapy (Ref 1), development antibiotic-loaded bone cement (Ref 2), progress in biomedical imaging and monitoring (Ref 3, 4), evolution of debridement and implant retention procedure (Ref 5), and the surge in the use of antibiotic-impregnated articulating spacers (Ref 6), the infection and osteomyelitis rates are still noteworthy with 4–64% in open long-bone fractures and about 1% in total joint replacements (TJR) (Ref 7). The by-products and debris produced due to the corrosion of implants lead to aseptic osteolysis, which accounts for almost two-thirds of TJR failures (Ref 8). CoCr alloys have been widely used as orthopedic implants, especially in TJR and in odontology, due to robust mechanical properties and lower wear in vivo compared to titanium alloys and stainless steels (Ref 9). However, the excessive release of ions, such as Co^{2+} , Cr^{3+} , and Cr^{6+} , from CoCr implants results in hypersensitivity and inflammatory reactions as well as chromosome breakage and DNA damage, cell apoptosis, and later necrosis (Ref 10, 11). HA ($\text{Ca}_{10}(\text{PO}_4)_6(\text{OH})_2$) coatings are considered as a promising method to prevent the excessive release of these ions (Ref 12, 13). HA has chemical and biological similarities to the human hard tissue (bone) (Ref 14, 15), and its coating can boost bone cell growth (i.e., osteoblast) activity which enhances the interaction between implant and the surrounding tissue (termed as “osseointegration”) (Ref 16). To improve the performance of CoCr

✉ Buta Singh Sidhu
butasidhu@yahoo.com

¹ Department of Mechanical Engineering, Punjabi University, Patiala, Punjab 147002, India

² MRS Punjab Technical University, Bathinda, Punjab 151001, India

alloys for biomedical applications, HA coating had been investigated in the earlier studies, in which HA coatings were mainly deposited by using electrochemical deposition, electrophoretic deposition, and sol-gel method (Ref 17-20). It is worthwhile to mention that plasma spraying is the only clinically accepted coating method for HA coating on a metallic substrate as well as it is commercially viable and a repeatable technique with high deposition efficiency (Ref 21). Various reinforcements such as silicon oxide (SiO_2), calcium phosphate (CaP), titanium oxide (TiO_2), zirconium oxide (ZrO_2), polycaprolactide (PCL), and zinc had been tried in HA coating to further enhance its performance for the bio-implant applications (Ref 22-25).

The clinical practices of the use of Ta as an implant started about half a century ago in a wide range of diagnostic and implant applications such as cranioplasty plates, orthopedic and dental implants, vascular clips and endovascular stent (Ref 26-29). However, relatively high cost and casting ability issues due to the complex shapes required were major obstacles in the acceptance of Ta as a bulk material for implants manufacturing (Ref 30, 31). This issue leads to a new approach of using Ta as a coating constituent for the surface modification of traditional biomaterials. Moreover, Ta in combination with HA is rarely studied compared to other materials formulations. By using Ta as a reinforcement in HA, the prominent cause of implant failure, i.e., corrosion (Ref 32), can be addressed at relatively low expense compared to a bulk Ta implant.

In addition to corrosion properties, the analysis of surface properties, such as surface hardness, roughness, and wettability, is also essential because these properties influence the corrosion resistance and biocompatibility. Surface hardness is a critical property, which is frequently associated with the surface degradation rate of implants (Ref 33). Surface roughness is often related to biocompatibility because attachment of the biomolecules and cell tissues depend upon the surface area provided by the implant (Ref 34). Generally, the rougher the surface, then the better will be the attachment of biomolecules and cell tissues. Surface wettability has attracted the attention of researchers due to its correlation with the biologic response of implants. The rate at which a surface is being hydrated decides its wettability. The rate and ease of attachment of biomolecules to the surface of an implant depend on the rate of surface hydration (Ref 35).

The results of corrosion behavior and surface property analyses of plasma-sprayed Ta-reinforced HA coating on CoCr alloy (ASTM F-1537) have not been reported. In this study, plasma-sprayed coatings of HA, Ta, HA reinforced with 10, 20, and 30 wt.% of Ta (HA-10Ta, HA-20Ta, and HA-30Ta) were developed on CoCr alloy. The corrosion behavior of uncoated and coated samples was investigated

using electrochemical corrosion testing along with surface property analyses.

Materials and Methods

Materials

A solid rod of CoCr alloy (ASTM F-1537) supplied by Zapp Precision Metals, Schwerte, Germany, was cut into $\Phi 15 \text{ mm} \times 5 \text{ mm}$ disks to form the substrate. These disks were then grit-blasted using alumina particles of size of 50-70 μm at a pressure of 5 bars to generate a rough surface followed by air blasting to remove any residual grit. Powders of HA (Medicoat, Etupes, France) and Ta (BGY Science and Technology Co. Ltd., Beijing, China) of particle size 45-125 μm were sprayed. The morphology of HA powder and Ta powder was determined by SEM (JEOL JSM-6610LV, Akishima, Japan) and is shown in Fig. 1. The morphology of the particles was irregular for both powders. The HA powder blended with Ta contents of 10, 20, and 30 wt.% was used as spray feedstock. To ensure the homogeneity of the mixtures, a jar mill (Mikrons, Chennai, India) was used for the blending process.

Deposition of Coatings

Coatings of HA, Ta, HA-10Ta, HA-20Ta, and HA-30Ta were produced using plasma spray processing at MEC Pvt. Ltd., Jodhpur, India. Plasma spray gun MF4 (MEC Pvt. Ltd., Jodhpur, India) was used for plasma spraying. The spraying parameters were: an arc voltage of 63 volts, arc

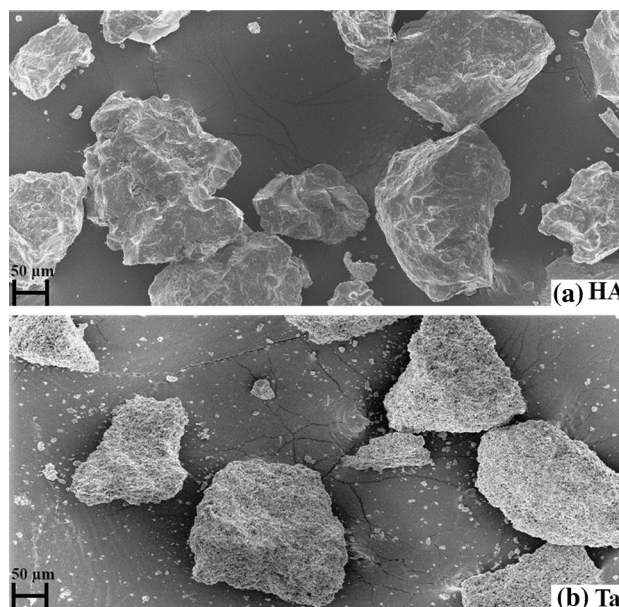


Fig. 1 Morphology of powders: (a) HA (b) Ta

current of 600 A, traverse speed of 10 mm/s, rotating speed 30 rpm, and six number of passes. The flow rate of the primary gas (argon) and secondary gas (hydrogen) was 40 SLPM and 5 SLPM, respectively. The standoff distance and distance between spray beads was maintained at 75 and 125 mm, respectively.

Characterization of Coatings

XRD analysis (X'Pert Pro PANalytical PN-3040/80, Almelo, the Netherlands) was undertaken to carry out the structural characterization of the coatings using the Cu-K α radiation ($\lambda = 0.15406$ nm) with 40 kV and 30 A, over a 2θ range of 20° – 80° . The crystallinity of the HA phase in the coatings was determined through Eq 1 as per an earlier study (Ref 36). In Eq 1, ΣA_{HA} is the total integrated area under HA peaks in 25° – 37° range of 2θ and ΣA_{T} is the total area under XRD pattern of 2θ range of 25° – 37° including the area under HA peaks as well as amorphous hump and peaks. The area was calculated using curve fitting and estimated relative error was within $\pm 2\%$ of the mean value

$$\text{Crystallinity (\%)} = \frac{\Sigma A_{\text{HA}}}{\Sigma A_{\text{T}}} \quad (\text{Eq 1})$$

Surface morphology and elemental composition of the coatings were analyzed before and after corrosion testing in Ringer's solution by using SEM equipped with EDX (JEOL JSM-6610LV, Akishima, Japan). Spot size (SS) 50 was used for EDX analysis. EDX elemental mapping of the exposed coated samples was carried out on cross sections to further observe the distribution of the compositional elements of the substrate as well as coatings. For elemental mapping analysis, the samples were cut across the cross section by using a low-speed precision saw and mounted in epoxy resin. To obtain a mirror finish, the samples were first polished by emery papers of grade 220, 320, 400, 800, 1000, and 2000, and then buffing of samples was done using alumina slurry on napped cloth. To achieve the desired conductivity, all the samples were coated with a thin layer of gold by using sputtering technique prior to SEM/EDX analysis.

Surface Properties

The microhardness of the surface was evaluated from the polished cross section of the coatings using a microhardness testing machine (Wolpert Wilson 402MVD, Aachen, Germany). For microhardness testing, 50 gf load was used for 15-s dwell time. The roughness of the surfaces was analyzed by using a surface roughness tester (Mitutoyo SJ-210, Kamasaki, Japan). Wettability of surface was evaluated from the contact angle measurement between Ringer's

solution droplet and the surface using a goniometer (First Ten Angstroms FTA2000, Portsmouth, USA). Fifteen readings of each surface property were taken and the average value is reported.

Electrochemical Corrosion Analysis

The corrosion behavior of the coated and uncoated samples was evaluated by using the potentiodynamic polarization technique. Electrochemical corrosion tests were conducted using a Potentiostat/Galvanostat/ZRA (Gamry G-750, Warminster, USA) with the standard three-electrode arrangement. Ag/AgCl (saturated KCl) and graphite rod served as reference and counter electrodes, respectively, while the uncoated/coated sample formed working electrode. For simulating human body fluid conditions, Ringer's solution (Nice Chemicals Pvt. Ltd., Kochi, India) was used as an electrolyte with the chemical composition (in gram/L) as 9 NaCl, 0.24 CaCl₂, 0.43 KCl, and 0.2 NaHCO₃ at pH 7.2. The potentiodynamic scan was performed from an initial potential of -0.25 V to the final potential of 0.25 V with respect to open-circuit potential at a scan rate of 0.5 mV/Sec. The potentiodynamic curve was then analyzed with Echem Analyst Software (Gamry Instruments, Warminster, USA) to acquire the values of electrochemical parameters by using Tafel extrapolation. Each sample was immersed in Ringer's solution for 24 h before conducting the experiments to obtain a relatively stable state. Only a surface area of 1 cm² was exposed to the Ringer's solution for each sample by covering all the other sides with epoxy. Testing of each sample was performed at least thrice to establish a good agreement between the curves.

Results and Discussion

XRD Analysis

The XRD patterns of the HA, Ta, HA-10Ta, HA-20Ta, and HA-30Ta powders are shown in Fig. 2. The XRD patterns reveal that both HA and Ta powders consisted of crystalline phases. The HA and Ta phases were compared with JCPDS card no. 9-432 and 4-788, respectively. With an increment of Ta content in HA powder, no negative effect on the crystallinity of HA phase was observed, while Ta peaks became more prominent.

The XRD patterns of the as-sprayed HA, Ta, HA-10Ta, HA-20Ta, and HA-30T coatings are shown in Fig. 3. The analysis of HA and Ta-reinforced HA coatings revealed the presence of amorphous calcium phosphates, i.e., tetracalcium phosphate [(Ca₄(PO₄)₂O), TTCP], α -tricalcium phosphate [(α -Ca₃(PO₄)₂), α -TCP] and β -tricalcium phosphate [(β -Ca₃(PO₄)₂), β -TCP]. The peaks of TTCP, α -TCP,

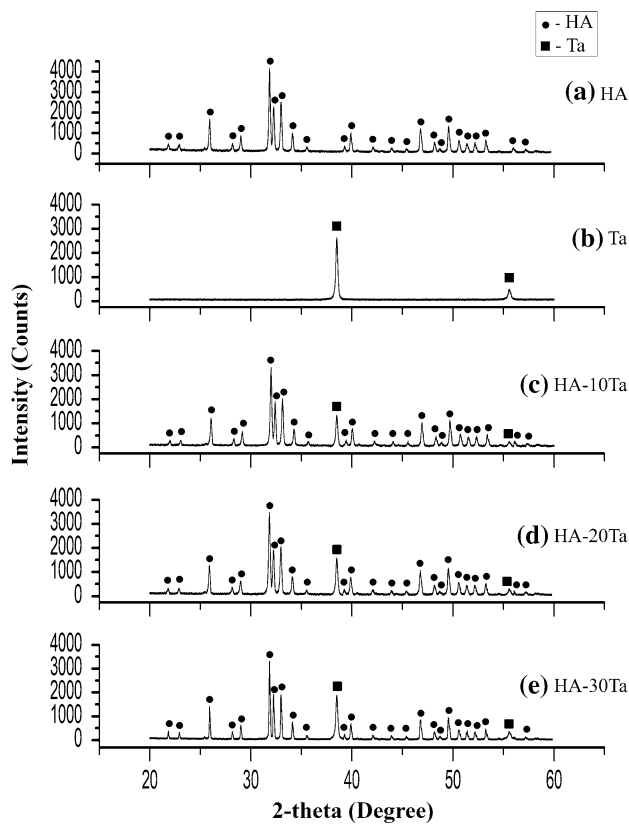


Fig. 2 XRD pattern of powders: (a) HA, (b) Ta, (c) HA-10Ta, (d) HA-20Ta, (e) HA-30Ta

and β -TCP were compared with JCPDS card no. 25-1137, 9-348 and 9-169, respectively. As plasma spraying involves processing at very high temperatures, amorphous phases of the feedstock powder are generally present in the coating (Ref 37).

In case of Ta and Ta-reinforced HA coatings, peaks corresponding to Ta oxide (JCPDS card no. 19-1300) were also observed. The earlier studies on Ta-based coatings, in which the coatings were deposited by using sol-gel method (Ref 38), electron beam melting (Ref 39), and anodization (Ref 40), suggested that the Ta oxide content in the coating was advantageous for the improved corrosion resistance and biological properties of the surface. When the Ta reinforcement increased in HA coating, the amorphous hump corresponding to β -TCP reduced and the peaks corresponding to TTCP lowered as well. The overall intensity of HA peaks slightly increases with increase in Ta reinforcement in HA. HA coating represented crystallinity of 74.6%, whereas HA-10Ta, HA-20Ta, and HA-30Ta coatings had a crystallinity of 78.7, 82.2 and 84.1%, respectively.

The difference in the thermal conductivities of HA and Ta could explain the change in crystallinity for the coatings. The thermal conductivity of Ta (57 W/m K) is about

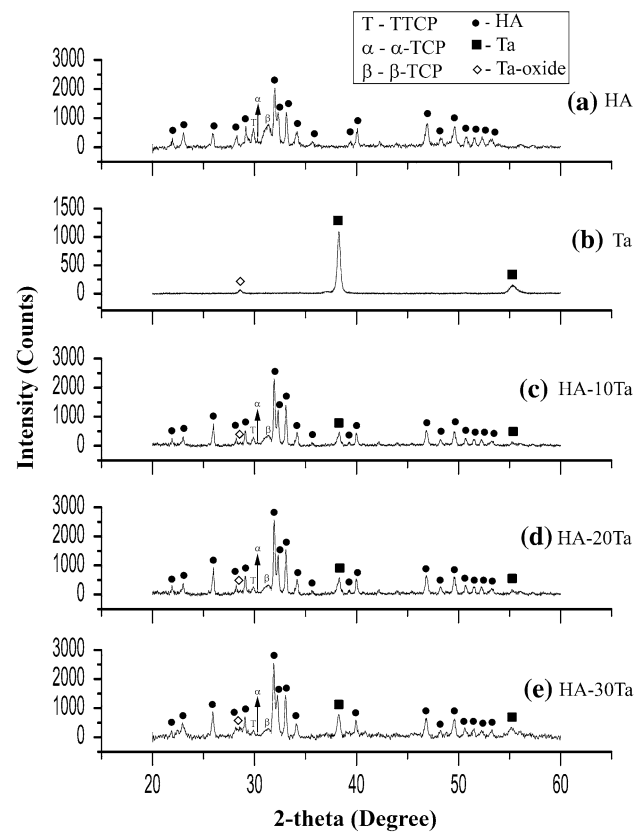


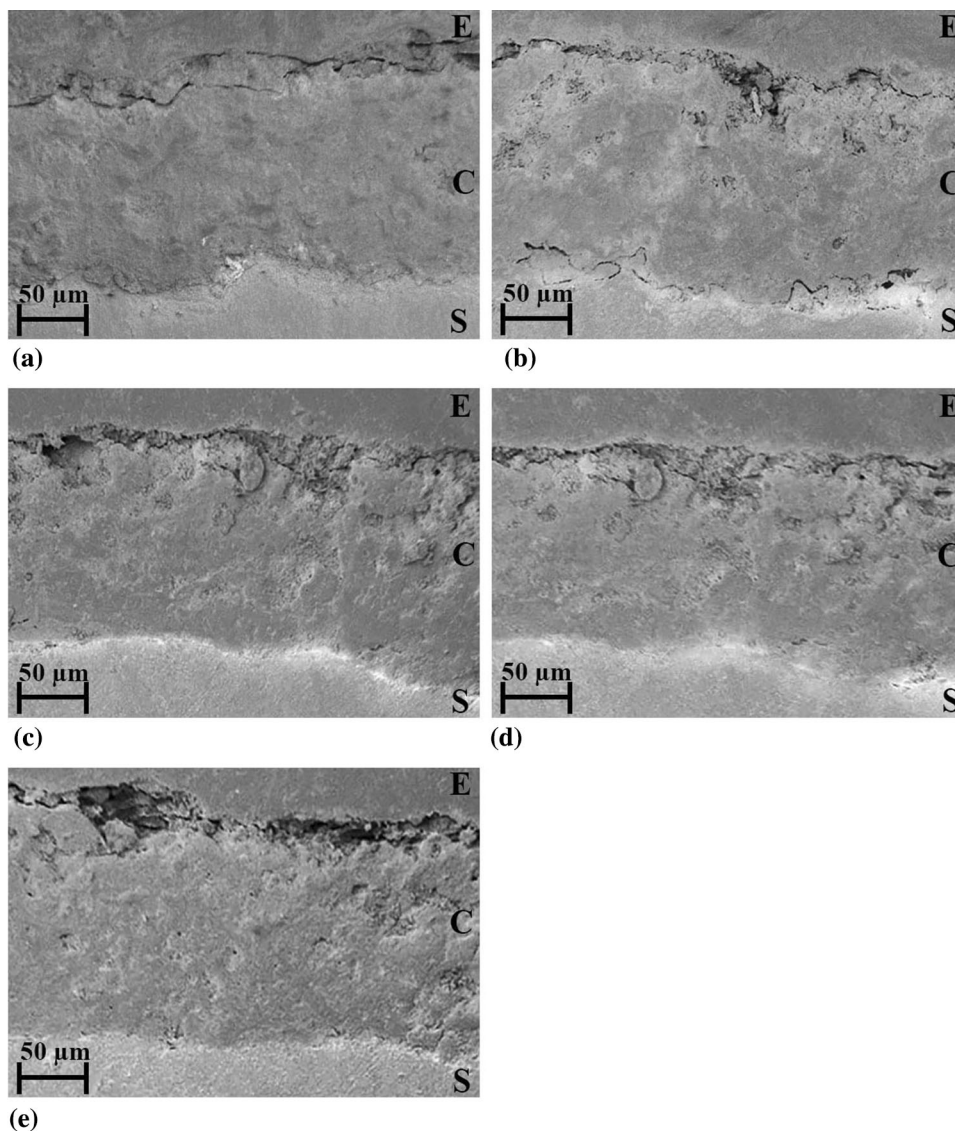
Fig. 3 XRD pattern of plasma-sprayed coatings on CoCr: (a) HA, (b) Ta, (c) HA-10Ta, (d) HA-20Ta, (e) HA-30Ta

81 times higher than HA (0.7 W/m K) (Ref 41, 42), which can create a thermal gradient across HA/Ta boundary. It is reported in the literature that when the thermal conductivity of the second constituent is significantly higher than HA, it allows the lower cooling rate to adjacent HA region/splats (Ref 43). Reportedly, rapid cooling rate is one of the main reasons due to which crystallinity of HA phase decreases after plasma spraying (Ref 44). Due to the presence of Ta, the slower cooling rate of the coating could be the reason for the higher crystallinity of HA phase for Ta-reinforced coatings.

SEM/EDX Analysis

Cross-sectional SEM analysis of as-sprayed HA, Ta, HA-10Ta, HA-20Ta, and HA-30Ta coatings are shown in Fig. 4. In this figure, the scanned area represents three domains, i.e., substrate (S), coating (C), and epoxy (E) domain. The average value of coating thickness measured from the SEM micrographs was around 125 μm . At the substrate-coating interface, no prominent crack was observed in case of HA coating. Similarly, Ta-reinforced HA coatings were also well adhered to the substrate and no major crack was observed at the substrate-coating

Fig. 4 SEM micrographs of plasma-sprayed coatings from interface with CoCr alloy substrate: (a) HA, (b) Ta, (c) HA-10Ta, (d) HA-20Ta, (e) HA-30Ta



interface. However, at the interface of Ta coating, some microcracks were noticed.

The SEM micrographs of as-sprayed HA, Ta, HA-10Ta, HA-20Ta, and HA-30Ta coatings are presented in Fig. 5. The morphology of HA coating (Fig. 5a) was dominated by spheroidized particles along with melt-resolidified fine and nodular particles over a small amount of accumulated splats. As the reinforcement of Ta increased in HA, the spheroidized particles decreased and the surface appeared to be constituted of well-flattened splats (Fig. 5c, d, and e). Some micropores were present on the surface of HA coating as well as on the Ta-reinforced HA coatings but no microcrack was observed. However, some micropore and microcracks were seen on the surface of the Ta coating (Fig. 5b). The reason for the development of microcracks at the interface and surface of the Ta coating could be the extremely anisotropic coefficients of thermal expansion of

Ta oxide, which can lead to spontaneous microcracking on cooling (Ref 45, 46). The EDX analysis of the HA coating revealed that the atomic calcium–phosphorus ratio (Ca/P) was 1.74. The Ca/P for HA-10Ta, HA-20Ta and HA-30Ta coatings were 1.72, 1.70 and 1.69, respectively. The Ca/P values exhibited by HA and Ta-reinforced HA coatings are within the ideal range of Ca/P (1.67–1.76) for HA-coated bio-implants (Ref 47). Further, the EDX analysis reveals a uniform distribution of reinforced Ta content in the HA coating without any lump formation.

Surface Properties Analysis

Surface Hardness

One of the key mechanical properties in determining the quality of the coating is microhardness (Ref 48). The

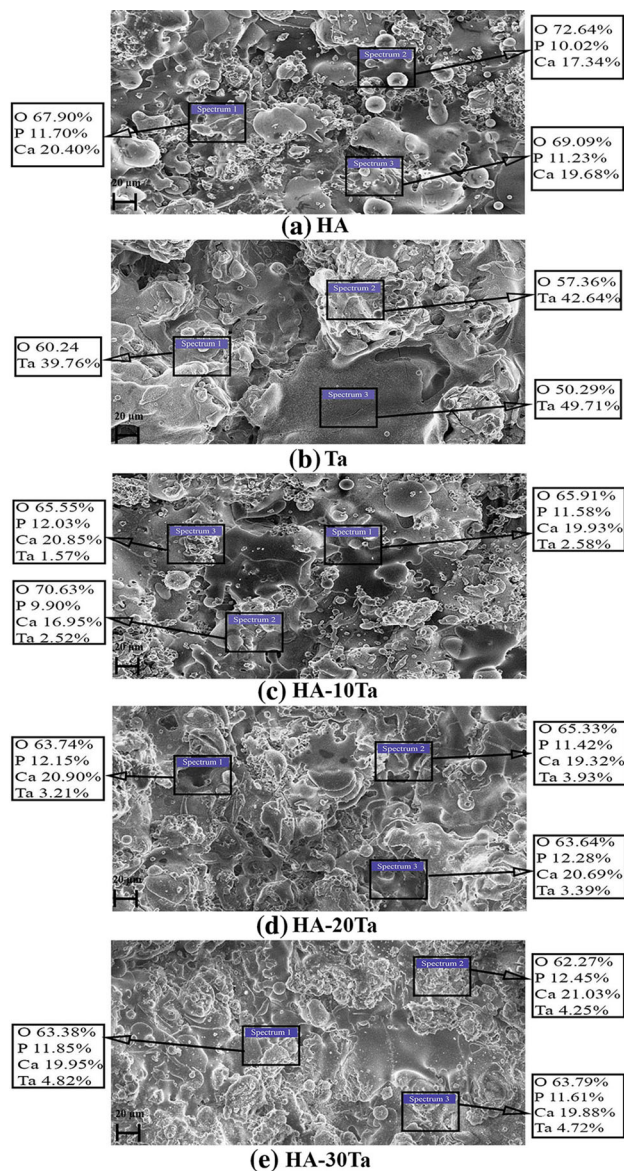
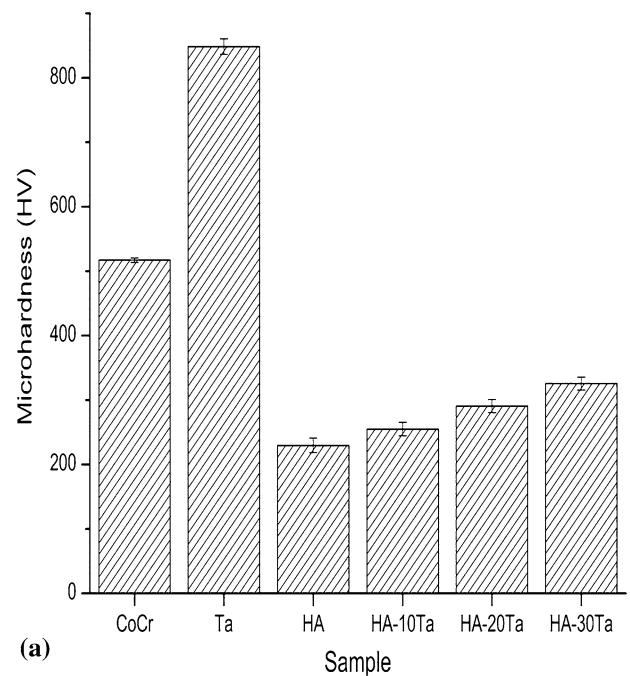
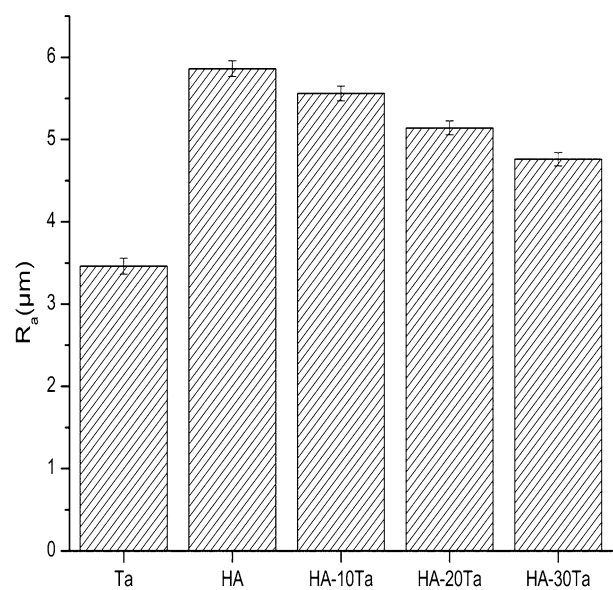


Fig. 5 SEM micrographs of plasma-sprayed coatings on CoCr: (a) HA, (b) Ta, (c) HA-10Ta, (d) HA-20Ta, (e) HA-30Ta

microhardness value of the samples is shown in Fig. 6(a). Microhardness of the uncoated CoCr alloy and Ta-coated surface was notably higher than the other samples. The HA-coated surface had the lowest microhardness value. As the reinforcement of Ta increased in the HA coating, the value of microhardness was enhanced significantly. The generation of the layered framework by the uniform distribution of reinforced Ta particles could be the reason for the increment in the surface hardness value for reinforced HA coatings. The previous studies conducted on reinforced HA coatings have also endorsed that the surface of the reinforced HA coating possessed higher surface hardness value than that of the pure HA coating (Ref 35, 49). The microhardness value for HA as well as Ta-reinforced HA



(a)



(b)

Fig. 6 (a) Microhardness values of samples, (b) R_a values for coated samples

coatings is comparable to the hardness value (200–300 HV) that the HA coatings generally exhibit (Ref 50).

Surface Roughness

The value of average surface roughness (R_a) of the uncoated CoCr alloy sample after air blasting was $1.16 \pm 0.2 \mu\text{m}$. The values of R_a for coated samples are depicted in Fig. 6(b). Ta-coated sample possessed the

lowest surface roughness. The R_a values of HA coating and HA-10Ta coating were very close. But in the case of HA-20 Ta and HA-30Ta samples, there was a noticeable decrease in the surface roughness as compared to HA coating. It can also be seen in the SEM micrographs (Fig. 5) that the surface seemed relatively flattened with lesser melt-resolidified particles as the Ta content increased in HA. The previous studies which analyzed the effect of surface finish on biocompatibility suggest that an adequately rough surface of the bio-implant improves protein absorption at the surface, which results in better cell tissue/bone adherence with the bio-implant (Ref 34, 51). The obtained values of surface roughness for HA and reinforced HA coating were within the range of surface roughness produced by plasmas-sprayed coatings ($R_a = 2\text{--}6\ \mu\text{m}$) as reported by Gross and Babovic (Ref 52).

Surface Wettability

The contact angle value and profile of Ringer’s solution droplet on the surface of different samples are shown in Fig. 7. The surface of the uncoated CoCr alloy was found to be of slightly hydrophobic nature. Ta coating also possessed hydrophobic nature, which is consistent with the previous studies conducted on Ta coating (Ref 53, 54). The nature of CoCr surface altered to hydrophilic with HA coating. With the Ta reinforcement in HA, a slight increase in the contact angle values was observed as compared to the HA-coated surface but the nature of the surface remained hydrophilic. Cells could be described as a simple viscous fluid during initial contact with the surface of an

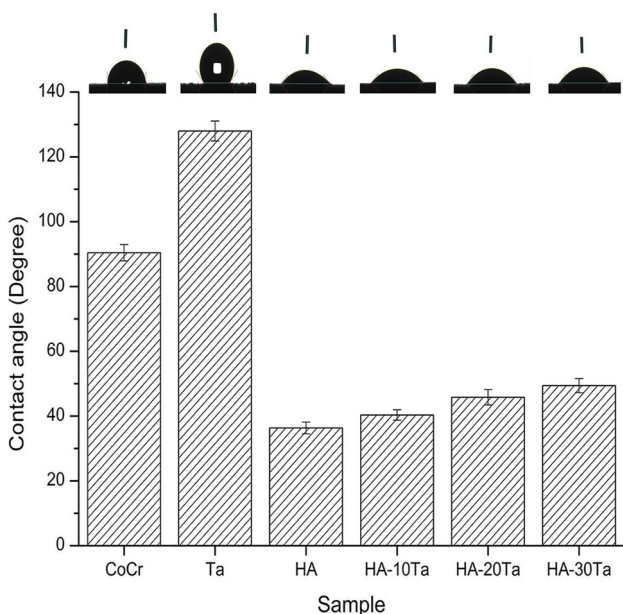


Fig. 7 Contact angle values for different samples

implant (Ref 55). After implantation, proteins from the blood (i.e., collagen, fibronectin, laminin, and vitronectin) are absorbed in the surface of an implant and then the cell attachment at the surface starts (Ref 56). A contact angle value of 60° or below was classed as hydrophilic and for the hydrophilic nature of the surface, cell adhesion found to be favored as per the literature (Ref 57).

Electrochemical Investigation

Potentiodynamic polarization curves of the uncoated CoCr, HA, Ta, HA-10Ta, HA-20Ta and HA-30Ta-coated samples are shown in Fig. 8. The corresponding electrochemical parameters, i.e., corrosion current density (I_{corr}), corrosion potential (E_{corr}), anodic slope (β_a), and cathodic slope (β_c) are enlisted in Table 1. E_{corr} and I_{corr} are very effective parameters to analyze and compare corrosion behavior of different samples in a specific solution under similar conditions. The E_{corr} value refers to the chemical potential of a material to corrosion, a nobler E_{corr} value represents higher corrosion protection ability (Ref 58). The I_{corr} value is a kinetic parameter to quantify the corrosion rate and lower I_{corr} value is an indication of higher corrosion resistance (Ref 59).

The E_{corr} value of uncoated CoCr alloy was the lowest and for coated samples, the order for E_{corr} value was: Ta < HA < HA-10Ta < HA-20Ta < HA-30 Ta. The Ta coating and HA coating improved the E_{corr} value of the uncoated CoCr and this value further shifted to nobler direction with Ta-reinforced HA coatings. The I_{corr} value of uncoated CoCr was the highest among all the samples. The Ta-coated samples revealed lower I_{corr} values than the uncoated sample but higher than HA coating. The results of electrochemical corrosion testing are in agreement with the earlier studies on HA-coated CoCr alloys which revealed that the corrosion resistance of uncoated specimens was improved by HA coating (Ref 18-20). The surface microcracks (Fig. 5b) present at the Ta coating could be the

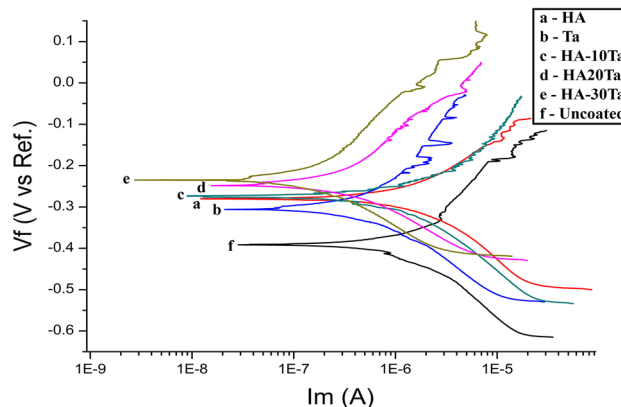


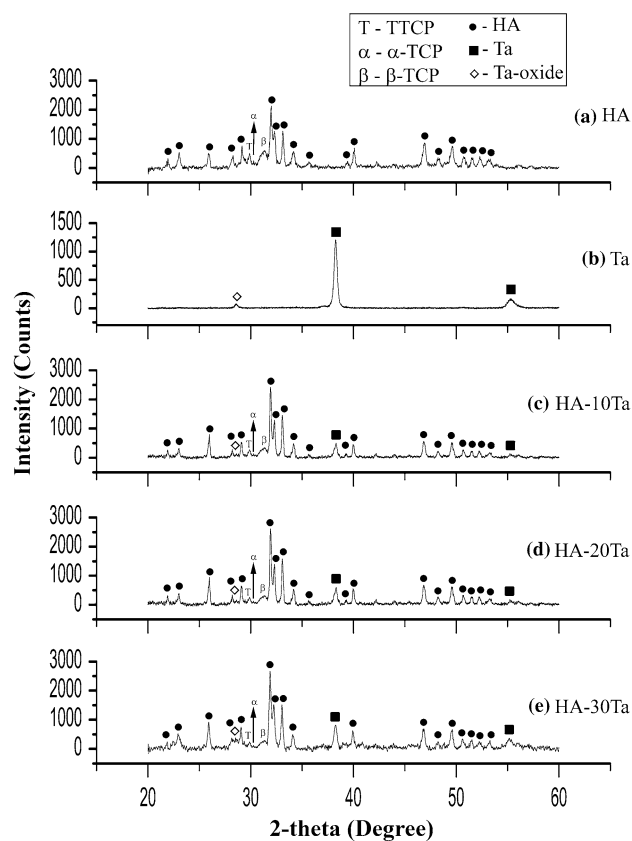
Fig. 8 Potentiodynamic polarization curves of different samples

Table 1 Corrosion parameters determined by Tafel Extrapolation method

Sample	E_{corr} , V	I_{corr} , A/cm ²	β_a , e ⁻³ V/decade	β_c , e ⁻³ V/decade
Uncoated CoCr	- 392	3.03E-06	166	143
Ta	- 306	415E-09	190	176
HA	- 280	354E-09	175	148
HA-10Ta	- 274	328E-09	149	162
HA-20Ta	- 254	269E-09	137	119
HA-30Ta	- 245	262E-09	141	122

reason for its lower E_{corr} and higher I_{corr} values than the HA coating. Any structural imperfection in the coating such as a microcrack facilitates corrosion under the coating or on the surface of the substrate, which leads to leaching of ions to the corrosive media and thus resulting in a decrease in protection ability/corrosion resistance of the surface (Ref 60). With the Ta reinforcement in HA, the I_{corr} value further decreased and HA-30Ta-coated sample exhibited lowest I_{corr} which is about 11.5 times lower than the uncoated CoCr alloy. Fathi and Azam (Ref 61) also reported that HA/Ta-coated specimen revealed to be significantly higher corrosion resistant than the bare stainless steel 316L. In the present study, the difference between the crystallinity of HA and Ta-reinforced HA coatings could explain the decrease in I_{corr} value, i.e., enhancement of corrosion resistance. Mohajernia et al. (Ref 62) reported that the higher phase purity of HA coating improves corrosion resistance as well as the biological performance of the bio-implants. The crystallinity of HA phase was increased with the incremental increase of Ta reinforcement in HA coating and consequently I_{corr} decreased. In addition, the surface roughness is also an important factor which influences the corrosion behavior of a surface. Dudin et al. (Ref 63) suggested that pit formation on the rougher surface can happen easier as compared to a smoother surface. The pit formation leads to pitting corrosion, which results in lower protection ability of the surface. The earlier studies also demonstrated that corrosion resistance decreases with increased surface roughness (Ref 22, 63, 64). It has been proved that the ions resulting from the corrosion of metallic implants may affect cell metabolism, i.e., cell behavior may be affected by corrosion current (Ref 61). In the present study, the Ta reinforcement enhanced the corrosion resistance as well as the crystallinity of HA coating which could improve the long-term survivability and osseointegration (Ref 65).

XRD patterns of coated samples after electrochemical corrosion testing are shown in Fig. 9. The analysis of XRD data revealed that all the coatings have maintained phase purity, i.e., no major phase appeared/disappeared after exposure to the Ringer's solution. However, a small increase in the overall peak intensities of HA as well as Ta-reinforced HA coatings was observed. The crystallinity

**Fig. 9** XRD pattern of plasma-sprayed coatings on CoCr alloy after corrosion testing: (a) HA, (b) Ta, (c) HA-10Ta, (d) HA-20Ta, (e) HA-30Ta

values of HA, HA-10Ta, HA-20Ta and HA-30Ta were 78.8, 80.2, 83.2, and 85.1%, respectively. A slight increase in the crystallinity value for the HA phase can be attributed to the dissolution of the amorphous phases during immersion in Ringer's solution. For the early stage in the development of biological equivalents that play a mediator role between osteoclast and osteoblast differentiation, the initial dissolution of HA is considered advantageous (Ref 37).

The surface morphology of the coated samples after corrosion testing is shown in Fig. 10. In the as-sprayed coating of HA, several spheroidized particles were present, but after corrosion testing, the microstructure mainly

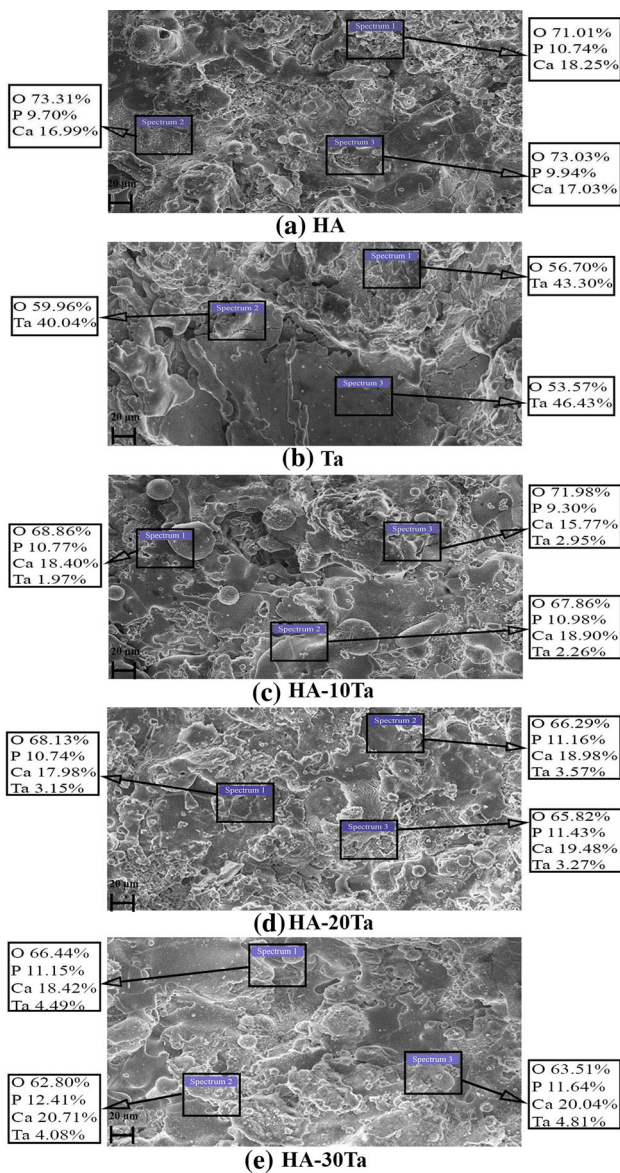


Fig. 10 SEM micrographs of plasma-sprayed coatings on CoCr alloy after corrosion testing: (a) HA, (b) Ta, (c) HA-10Ta, (d) HA-20Ta, (e) HA-30Ta

consisted of accumulated splats and some flattened particles of irregular morphology (Fig. 10a). Some microcracks were also observed on the surface of the HA-coated sample after corrosion testing. The microcracks that were present on as-sprayed Ta-coated surface became more noticeable after exposure to Ringer’s solution (Fig. 10b). The microstructure of HA-10Ta, HA-20Ta and HA-30Ta sample (Fig. 10c, d, and e, respectively) consisted of well-flattened splats and free from any prominent microcrack after corrosion testing. Presence of a microcrack in the coating leads to a decrease in corrosion protection ability of the surface but more importantly, it can cause coating failure/delamination (Ref 44, 66).

To detect the changes in the composition of the coating, if any, EDX analysis was carried out after electrochemical corrosion testing. EDX data revealed that the Ca:P decreased for HA as well as Ta-reinforced HA-coated samples after exposure to Ringer’s solution. The value of Ca/P for HA, HA-10Ta, HA-20Ta, and HA-30Ta coatings were 1.72, 1.70, 1.69, and 1.68, respectively. The oxygen content for HA-, HA-10Ta-, HA-20Ta-, and HA-30Ta-coated samples was observed to be increased from 69.9, 67.4, 64.2, and 63.1% to 72.4, 69.6, 66.7, and 64.3%, respectively. The increase in oxygen content and a decrease in Ca:P after immersion in Ringer’s solution/simulated body fluid as observed in the present investigation was also reported in the earlier studies conducted on HA (Ref 15, 22, 66). The increased oxygen content of the coating can also enhance the attachment of biomolecules to the surface of bio-implant (Ref 59).

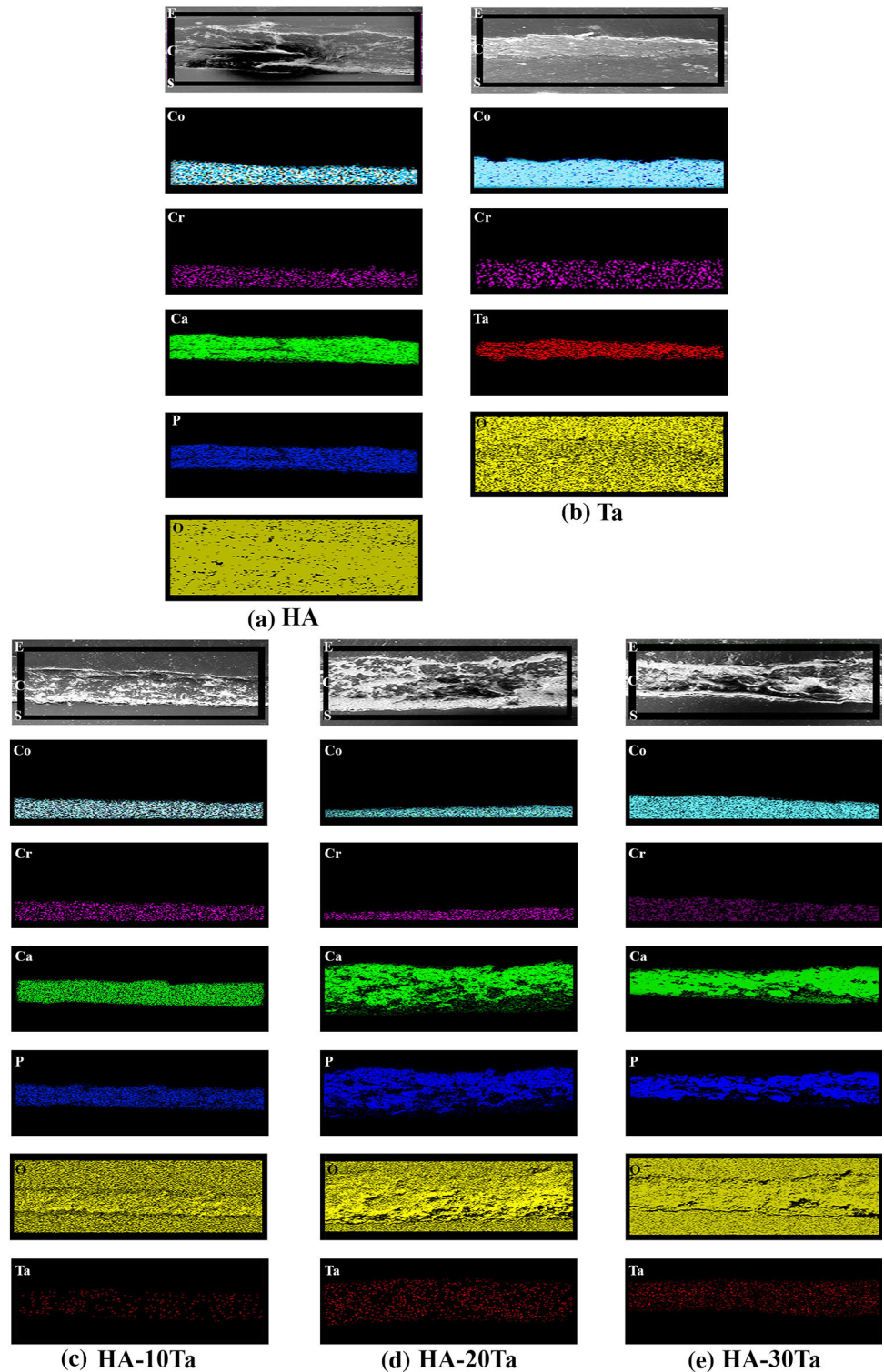
EDX elemental mapping of the cross section of the coated samples after electrochemical corrosion testing is presented in Fig. 11. In all the coatings, no constituent of the substrate’s composition was observed in the coating domain. The major coating constituents of HA coating, i.e., Ca and P along with Ta in the case of Ta-reinforced HA coatings were distributed uniformly over the coating domain. The results of SEM/EDX analysis from the surface and elemental mapping from cross section after corrosion testing revealed that the Ta-reinforced HA coatings retained their morphology and compositional integrity even after corrosion testing.

Conclusions

In this study, the coatings of HA, Ta, HA-10Ta, HA-20Ta, and HA-30Ta were successfully developed over CoCr alloy by using plasma spraying technique. The characterization of the coatings has been done on the basis of microstructure, phase composition, corrosion behavior, and surface properties. The following conclusions have been drawn from the study:

- The Ta-reinforced HA coatings demonstrated better crystallinity than pure HA coating and fraction of amorphous phases decreases with the increase in Ta content in the coating.
- The surface of as-sprayed HA coating and Ta-reinforced HA coatings found to be free from any microcrack and a sound and adherent interface between substrate and coating was observed. However, microcracks were present on the surface as well as at the substrate-coating interface of the pure Ta coating.
- With the increase in Ta reinforcement in HA coating, microhardness of the surface increased significantly.

Fig. 11 Elemental mapping of plasma-sprayed coatings on CoCr alloy after corrosion testing: (a) HA, (b) Ta, (c) HA-10Ta, (d) HA-20Ta, (e) HA-30Ta



However, lower surface roughness was observed in case of Ta-reinforced HA coatings as compared to the pure HA coating.

- The surfaces of the CoCr alloy, as well as Ta coating, were hydrophobic. HA-coated surface nature revealed hydrophilic nature. With the Ta reinforcement, the

contact angles between Ringer's solution droplet and the surface increased slightly, but the nature of the surface remained hydrophilic.

- The corrosion resistance uncoated CoCr alloy was enhanced by pure HA coating as well as Ta-reinforced HA coatings, whereas Ta-coated sample demonstrated

relatively lower corrosion resistance as compared to other coated samples. A decrease in the I_{corr} for the Ta-reinforced HA coatings was observed (~ 7 , 24 and 26% for HA-10Ta, HA-20Ta, and HA-30Ta, respectively) as compared to the HA coating.

- After exposure to Ringer's solution, the microcracks which were present in the as-sprayed Ta coating became more prominent and some microcracks were observed on the surface of HA coating. Ta-reinforced HA coatings effectively maintained the morphological integrity confirming their superior protection ability.

These findings provide a perspective of Ta-reinforced HA coatings for improving the corrosion resistance as well as surface properties, which may be a promising combination for CoCr based bio-implants and deserves further biological investigation.

Acknowledgments The authors would like to express gratitude to Medicoat, France and Zapp Precision Metals, Germany for sponsoring HA power and CoCr alloy substrates, respectively. The authors would also like to express gratitude to Mechanical Engineering Department, IIT Ropar, India, for providing research facilities for corrosion and surface analysis for this research work.

References

1. D.R. Osmon, E.F. Berbari, A.R. Berendt, D. Lew, W. Zimmerli, J.M. Steckelberg, N. Rao, A. Hanssen, W.R. Wilson, and Infectious Diseases Society of America, Diagnosis and Management of Prosthetic Joint Infection: Clinical Practice Guidelines by the Infectious Diseases Society of America, *Clin. Infect. Dis.*, 2013, **56**(1), p e1-e25
2. K. Anagnostakos, Therapeutic Use of Antibiotic-Loaded Bone Cement in the Treatment of Hip and Knee Joint Infections, *J. Bone Jt. Infect.*, 2017, **2**(1), p 29-37
3. A. Marro, T. Bandukwala, and W. Mak, Three-Dimensional Printing and Medical Imaging: A Review of the Methods and Applications, *Curr. Probl. Diagn. Radiol.*, 2016, **45**(1), p 2-9
4. A. Taruttis and V. Ntziachristos, Advances in Real-Time Multispectral Optoacoustic Imaging and Its Applications, *Nat. Photonics*, 2015, **9**(4), p 219-227
5. C.L. Abad and A. Haleem, Prosthetic Joint Infections: An Update, *Curr. Infect. Dis. Rep.*, 2018, **20**(7), p 15
6. O.J. Diamond and B.A. Masri, Articulating Antibiotic Impregnated Spacers in Prosthetic Joint Infections: Where Do We Stand?, *International Journal of Surgery*, 2018, **54**, p 345-350
7. G. Hu, L. Zeng, H. Du, X. Fu, X. Jin, M. Deng, Y. Zhao, and X. Liu, The Formation Mechanism and Bio-Corrosion Properties of Ag/HA Composite Conversion Coating on the Extruded Mg-2Zn-1Mn-0.5Ca Alloy for Bone Implant Application, *Surface Coat. Technol.*, 2017, **325**, p 127-135
8. N.J. Hallab and J.J. Jacobs, Biologic Effects of Implant Debris, *Bull. NYU Hosp. Jt. Dis.*, 2009, **67**(2), p 182-188
9. C. Balagna, M.G. Faga, and S. Spriano, Tantalum-Based Multilayer Coating on Cobalt Alloys in Total Hip and Knee Replacement, *Mater. Sci. Eng. C*, 2012, **32**(4), p 887-895
10. A.G. Cobb and T.P. Schmalzreid, The Clinical Significance of Metal Ion Release from Cobalt-Chromium Metal-on-Metal Hip Joint Arthroplasty, *Proc. Inst. Mech. Eng. H*, 2006, **220**(2), p 385-398
11. L. Luo, A. Petit, J. Antoniou, D.J. Zukor, O.L. Huk, R.C.W. Liu, F.M. Winnik, and F. Mwale, Effect of Cobalt and Chromium Ions on MMP-1, TIMP-1, and TNF- α Gene Expression in Human U937 Macrophages: A Role for Tyrosine Kinases, *Biomaterials*, 2005, **26**(28), p 5587-5593
12. D.Y. Lin and X.X. Wang, Electrodeposition of Hydroxyapatite Coating on CoNiCrMo Substrate in Dilute Solution, *Surf. Coat. Technol.*, 2010, **204**(20), p 3205-3213
13. S.B. Goodman, Z. Yao, M. Keeney, and F. Yang, The Future of Biologic Coatings for Orthopaedic Implants, *Biomaterials*, 2013, **34**(13), p 3174-3183
14. M.M. Taheri, M.R. Abdul Kadir, T. Shokuhfar, A. Hamlekhan, M. Assadian, M.R. Shirdar, and A. Mirjalili, Surfactant-Assisted Hydrothermal Synthesis of Fluoridated Hydroxyapatite Nanorods, *Ceram. Int.*, 2015, **41**(8), p 9867-9872
15. G. Singh, H. Singh, and B.S. Sidhu, Characterization and Corrosion Resistance of Plasma Sprayed HA and HA-SiO₂ Coatings on Ti-6Al-4V, *Surf. Coat. Technol.*, 2013, **228**, p 242-247
16. M. Vallet-Regí and J.M. González-Calbet, Calcium Phosphates as Substitution of Bone Tissues, *Prog. Solid State Chem.*, 2004, **32**(1), p 1-31
17. T. Moskalewicz, A. Łukaszczyk, A. Kruk, M. Kot, D. Jugowicz, B. Dubiel, and A. Radziszewska, Porous HA and Nanocomposite Nc-TiO₂/HA Coatings to Improve the Electrochemical Corrosion Resistance of the Co-28Cr-5Mo Alloy, *Mater. Chem. Phys.*, 2017, **199**, p 144-158
18. M. Ibrahim Coşkun, İ.H. Karahan, and Y. Yücel, Optimized Electrodeposition Concentrations for Hydroxyapatite Coatings on CoCrMo Biomedical Alloys by Computational Techniques, *Electrochim. Acta*, 2014, **150**, p 46-54
19. M.R. Shirdar, S. Izman, M.M. Taheri, M. Assadian, and M.R.A. Kadir, Effect of Electrophoretic Deposition Parameters on the Corrosion Behavior of Hydroxyapatite-Coated Cobalt-Chromium Using Response Surface Methodology, *Arab. J. Sci. Eng.*, 2016, **41**(2), p 591-598
20. H. Kheimehsari, S. Izman, and M.R. Shirdar, Effects of HA-Coating on the Surface Morphology and Corrosion Behavior of a Co-Cr-Based Implant in Different Conditions, *J. Mater. Eng. Perform.*, 2015, **24**(6), p 2294-2302
21. A.A. Campbell, Bioceramics for Implant Coatings, *Mater. Today*, 2003, **6**(11), p 26-30
22. G. Singh, H. Singh, and B.S. Sidhu, Corrosion Behavior of Plasma Sprayed Hydroxyapatite and Hydroxyapatite-Silicon Oxide Coatings on AISI, 304 for Biomedical Application, *Appl. Surf. Sci.*, 2013, **284**, p 811-818
23. G. Singh, H. Singh, and B.S. Sidhu, In Vitro Corrosion Investigations of Plasma-Sprayed Hydroxyapatite and Hydroxyapatite-Calcium Phosphate Coatings on 316L SS, *Bull. Mater. Sci.*, 2014, **37**(6), p 1519-1528
24. Y. Huang, X. Zhang, H. Qiao, M. Hao, H. Zhang, Z. Xu, X. Zhang, X. Pang, and H. Lin, Corrosion Resistance and Cytocompatibility Studies of Zinc-Doped Fluorohydroxyapatite Nanocomposite Coatings on Titanium Implant, *Ceram. Int.*, 2016, **42**(1, Part B), p 1903-1915
25. A. Abdal-hay, N.A.M. Barakat, and J.K. Lim, Hydroxyapatite-Doped Poly(Lactic Acid) Porous Film Coating for Enhanced Bioactivity and Corrosion Behavior of AZ31 Mg Alloy for Orthopedic Applications, *Ceram. Int.*, 2013, **39**(1), p 183-195
26. G.L. Burke, The Corrosion of Metals in Tissues; and an Introduction to Tantalum, *Can. Med. Assoc. J.*, 1940, **43**(2), p 125-128
27. C.B. Johansson, H.A. Hansson, and T. Albrektsson, Qualitative Interfacial Study between Bone and Tantalum, Niobium or Commercially Pure Titanium, *Biomaterials*, 1990, **11**(4), p 277-280

28. J. Black, Biologic Performance of Tantalum, *Clin. Mater.*, 1994, **16**(3), p 167-173
29. B.R. Levine, S. Sporer, R.A. Poggie, C.J. Della Valle, and J.J. Jacobs, Experimental and Clinical Performance of Porous Tantalum in Orthopedic Surgery, *Biomaterials*, 2006, **27**(27), p 4671-4681
30. T. Albrektsson and A. Wennerberg, Oral Implant Surfaces: Part 2—Review Focusing on Clinical Knowledge of Different Surfaces, *Int. J. Prosthodont.*, 2004, **17**(5), p 544-564
31. V.K. Balla, S. Banerjee, S. Bose, and A. Bandyopadhyay, Direct Laser Processing of a Tantalum Coating on Titanium for Bone Replacement Structures, *Acta Biomater.*, 2010, **6**(6), p 2329-2334
32. U. Kamachimudali, T.M. Sridhar, and B. Raj, Corrosion of Bio Implants, *Sadhana*, 2003, **28**(3–4), p 601-637
33. A. Biswas, L. Li, T.K. Maity, U. Chatterjee, B.L. Moidike, I. Manna, and J. Majumdar, Laser Surface Treatment of Ti-6Al-4 V for Bio-Implant Application, *Lasers Eng.*, 2007, **17**, p 59-73
34. D. Yamashita, M. Machigashira, M. Miyamoto, H. Takeuchi, K. Noguchi, Y. Izumi, and S. Ban, Effect of Surface Roughness on Initial Responses of Osteoblast-Like Cells on Two Types of Zirconia, *Dent. Mater. J.*, 2009, **28**(4), p 461-470
35. D. Gopi, A. Karthika, D. Rajeswari, L. Kavitha, R. Pramod, and J. Dwivedi, Investigation on Corrosion Protection and Mechanical Performance of Minerals Substituted Hydroxyapatite Coating on HELCDEB-Treated Titanium Using Pulsed Electrodeposition Method, *RSC Adv.*, 2014, **66**(4), p 34751-34759
36. L. Sun, C.C. Berndt, and C.P. Grey, Phase, Structural and Microstructural Investigations of Plasma Sprayed Hydroxyapatite Coatings, *Mater. Sci. Eng. A*, 2003, **360**(1), p 70-84
37. W. Xue, S. Tao, X. Liu, X. Zheng, and C. Ding, In Vivo Evaluation of Plasma Sprayed Hydroxyapatite Coatings Having Different Crystallinity, *Biomaterials*, 2004, **25**(3), p 415-421
38. C. Arnould, C. Volcke, B. Lamarque, P.A. Thiry, J. Delhalle, and Z. Mekhalif, Titanium Modified with Layer-by-Layer Sol–Gel Tantalum Oxide and an Organodiphosphonic Acid: A Coating for Hydroxyapatite Growth, *J. Colloid Interface Sci.*, 2009, **336**(2), p 497-503
39. N. Donkov, A. Zykova, V. Safonov, R. Rogowska, J. Smolik, and V. Luk'yanchenko, Tantalum Pentoxide Ceramic Coatings Deposition on Ti4Al6 V Substrates for Biomedical Applications, *Prob. Atomic Sci. Tech.*, 2011, **1**, p 131-133
40. R.S. Namur, K.M. Reyes, C.E.B. Marino, R.S. Namur, K.M. Reyes, and C.E.B. Marino, Growth and Electrochemical Stability of Compact Tantalum Oxides Obtained in Different Electrolytes for Biomedical Applications, *Mater. Res.*, 2015, **18**, p 91-97
41. A. Rapacz-Kmita, A. Ślórsarczyk, Z. Paszkiewicz, and D. Paluch, Evaluation of HAp-ZrO₂ Composites and Monophase HAp Bioceramics. Vitro Study, *J. Mater. Sci.*, 2004, **39**(18), p 5865-5867
42. N.D. Milošević, G.S. Vuković, D.Z. Pavičić, and K.D. Maglić, Thermal Properties of Tantalum Between 300 and 2300 K, *Int. J. Thermophys.*, 1999, **20**(4), p 1129-1136
43. J.E. Tercero, S. Namin, D. Lahiri, K. Balani, N. Tsoukias, and A. Agarwal, Effect of Carbon Nanotube and Aluminum Oxide Addition on Plasma-Sprayed Hydroxyapatite Coating's Mechanical Properties and Biocompatibility, *Mater. Sci. Eng. C*, 2009, **29**(7), p 2195-2202
44. L. Sun, C.C. Berndt, K.A. Gross, and A. Kucuk, Material Fundamentals and Clinical Performance of Plasma-Sprayed Hydroxyapatite Coatings: A Review, *J. Biomed. Mater. Res.*, 2002, **58**(5), p 570-592
45. M. Moldovan, C.M. Weyant, D.L. Johnson, and K.T. Faber, Tantalum Oxide Coatings as Candidate Environmental Barriers, *J. Therm. Spray Tech.*, 2004, **13**(1), p 51-56
46. Y.W. Bae, W.Y. Lee, and D.P. Stinton, Effects of Temperature and Reagent Concentration on the Morphology of Chemically Vapor Deposited β -Ta₂O₅, *J. Am. Ceram. Soc.*, 1995, **78**(5), p 1297-1300
47. C. Auclair-Daigle, M.N. Bureau, J.-G. Legoux, and L'.H. Yahia, Bioactive Hydroxyapatite Coatings on Polymer Composites for Orthopedic Implants, *J. Biomed. Mater. Res. Part A*, 2005, **73**(4), p 398-408
48. M.F. Hasan, J. Wang, and C. Berndt, Determination of the Mechanical Properties of Plasma-Sprayed Hydroxyapatite Coatings Using the Knoop Indentation Technique, *J. Therm. Spray Tech.*, 2015, **24**(5), p 865-877
49. G. Singh, S. Singh, and S. Prakash, Surface Characterization of Plasma Sprayed Pure and Reinforced Hydroxyapatite Coating on Ti6Al4 V Alloy, *Surf. Coat. Technol.*, 2011, **205**(20), p 4814-4820
50. M.F. Hasan, J. Wang, and C. Berndt, Evaluation of the Mechanical Properties of Plasma Sprayed Hydroxyapatite Coatings, *Appl. Surf. Sci.*, 2014, **303**, p 155-162
51. F.A. Shah, M.L. Johansson, O. Omar, H. Simonsson, A. Palmquist, and P. Thomsen, Laser-Modified Surface Enhances Osseointegration and Biomechanical Anchorage of Commercially Pure Titanium Implants for Bone-Anchored Hearing Systems, *PLoS ONE*, 2016, **11**(6), p e0157504
52. K.A. Gross and M. Babovic, Influence of Abrasion on the Surface Characteristics of Thermally Sprayed Hydroxyapatite Coatings, *Biomaterials*, 2002, **23**(24), p 4731-4737
53. X. Yu, L. Tan, H. Yang, and K. Yang, Surface Characterization and Preparation of Ta Coating on Ti6Al4 V Alloy, *J. Alloys Compd.*, 2015, **644**, p 698-703
54. C.F. Almeida Alves, A. Cavaleiro, and S. Carvalho, Bioactivity Response of Ta_{1-x}O_x Coatings Deposited by Reactive DC Magnetron Sputtering, *Mater. Sci. Eng. C*, 2016, **58**, p 110-118
55. Z. Geng, R. Wang, X. Zhuo, Z. Li, Y. Huang, L. Ma, Z. Cui, S. Zhu, Y. Liang, Y. Liu, H. Bao, X. Li, Q. Huo, Z. Liu, and X. Yang, Incorporation of Silver and Strontium in Hydroxyapatite Coating on Titanium Surface for Enhanced Antibacterial and Biological Properties, *Mater. Sci. Eng. C*, 2017, **71**, p 852-861
56. F. Marashi-Najafi, J. Khalil-Allafi, and M.R. Etminanfar, Biocompatibility of Hydroxyapatite Coatings Deposited by Pulse Electrodeposition Technique on the Nitinol Superelastic Alloy, *Mater. Sci. Eng. C*, 2017, **76**, p 278-286
57. S. Durdu, K. Korkmaz, S.L. Aktuğ, and A. Çakır, Characterization and Bioactivity of Hydroxyapatite-Based Coatings Formed on Steel by Electro-Spark Deposition and Micro-Arc Oxidation, *Surf. Coat. Technol.*, 2017, **326**, p 111-120
58. M. Poorraeisi and A. Afshar, The Study of Electrodeposition of Hydroxyapatite-ZrO₂-TiO₂ Nanocomposite Coatings on 316 Stainless Steel, *Surf. Coat. Technol.*, 2018, **339**, p 199-207
59. H. Wang, Y. Zheng, C. Jiang, Y. Li, and Y. Fu, In Vitro Corrosion Behavior and Cytocompatibility of Pure Fe Implanted with Ta, *Surf. Coat. Technol.*, 2017, **320**, p 201-205
60. S.R. Kiahosseini, A. Afshar, M. Mojtahedzadeh Larjani, and M. Yousefpour, Structural and Corrosion Characterization of Hydroxyapatite/Zirconium Nitride-Coated AZ91 Magnesium Alloy by Ion Beam Sputtering, *Appl. Surface Sci.*, 2017, **401**, p 172-180
61. M.H. Fathi and F. Azam, Novel Hydroxyapatite/Tantalum Surface Coating for Metallic Dental Implant, *Mater. Lett.*, 2007, **61**(4), p 1238-1241
62. S. Mohajernia, S. Pour-Ali, S. Hejazi, M. Saremi, and A.-R. Kiani-Rashid, Hydroxyapatite Coating Containing Multi-walled Carbon Nanotubes on AZ31 Magnesium: Mechanical-Electrochemical Degradation in a Physiological Environment, *Ceram. Int.*, 2018, **44**(7), p 8297-8305
63. S. Dudin, C.M. Cotrut, M. Dinu, A. Zykova, A.C. Parau, S. Yakovlev, and A. Vladescu, Comparative Study of the

- Hydroxyapatite Coatings Prepared with/Without Substrate Bias, *Ceram. Int.*, 2017, **43**(17), p 14968-14975
64. R. Walter and M.B. Kannan, Influence of Surface Roughness on the Corrosion Behaviour of Magnesium Alloy, *Mater. Des.*, 2011, **32**(4), p 2350-2354
65. T.P.S. Sarao, H. Singh, and H. Singh, Enhancing Biocompatibility and Corrosion Resistance of Ti-6Al-4 V Alloy by Surface Modification Route, *J. Therm. Spray Tech.*, 2018, <https://doi.org/10.1007/s11666-018-0746-7>
66. Z. Zhang, M.F. Dunn, T.D. Xiao, A.P. Tomsia, and E. Saiz, Nanostructured Hydroxyapatite Coatings for Improved Adhesion and Corrosion Resistance for Medical Implants, *MRS Online Proc. Libr. Arch.*, 2001, **703**, p 291-296